Turkish Journal of Physics

http://journals.tubitak.gov.tr/physics/

Research Article

Turk J Phys
(2019) 43: 324 – 336
© TÜBİTAK
doi:10.3906/fiz-1807-39

The novel synthesis and luminescence studies of CuO and Fe_2O_3 embedded (8-hydroxyquinoline)zinc nanocomposites

Abraham Kutticheril EAPEN[1,*], **Paulose THOMAS**[2]
[1]Department of Physics, St. Berchmans College, Changanacherry, Kerala, India
[2]Department of Physics, Mar Thoma College for Women, Perumbavoor, Kerala, India

Received: 17.07.2018 • **Accepted/Published Online:** 11.03.2019 • **Final Version:** 02.08.2019

Abstract: The present study investigates the synthesis of novel luminescent polymer nanocomposite through the incorporation of CuO and Fe_2O_3 into a $C_{18}H_{12}N_2O_2Zn$ host polymer matrix. The observed green electroluminescence behavior originates mainly from the shift in the HOMO-LUMO energy gap of the polymer matrix caused by the inclusion of oxidized metal/oxygen ions from the incorporated metal oxides into the pyridyl and phenyl groups of the host polymer. The existence of oxidized metal/oxygen ionic states in the polymer matrix is successfully confirmed through X-ray photoelectron spectroscopic analysis. The FTIR analysis is utilized to verify the presence of pyridyl and phenyl groups in the host polymer matrix. The successful incorporation of CuO and Fe_2O_3 into the host polymer matrix is examined through FESEM and HRTEM analyses. XRD, EDS, and XPS analyses are employed in order to confirm the exact crystalline phase and material compositions of the samples prepared.

Key words: Metal oxide-(8-hydroxyquinoline)zinc polymer nanocomposites, organic photoelectroluminescence, morphology, XPS analysis

1. Introduction

For the past few years, researchers have focused their attention on the synthesis and characterization of light-emitting organic compounds for promising applications in various types of electroluminescent (EL) devices. Organic EL devices are supreme candidates for use in portable display device applications because of their lower power consumption and potential for the production of all ranges of color emissions [1–5]. Numerous EL studies have been conducted on metal-based quinoline derivatives such as tris-(8-hydroxyquinoline) aluminum (Alq_3), bis-(8-hydroxyquinoline), and zinc (Znq_2) due to their excellent flexibility, high photoconductivity, and the high lifespan of devices. As compared to Alq_3, Znq_2 has been used more extensively due to its efficient electron transport property, lower biasing voltages, and higher quantum yields in device performance [4–6]. For example, the comparative studies conducted by Huo et al. on organic light-emitting diode (OLED) performances of chloro and fluoro substituted Zn(II)8-hydroxyquinolinates found that the material is suitable for yellow OLEDs [7]. Sapochak et al. studied the EL and structural effects of zinc(II) bis(8-hydroxyquinoline) on electronic states and device performance. The study observed that the strategic substitution of 8-hydroxyquinoline ligands into the metal component and control of the structural symmetry of the corresponding metal chelates may offer a route to high efficiency and lower operating voltage for small-molecule OLEDs [8]. Wang et al. fabricated EL and phosphorescent OLEDs using novel Zn(II) complexes of 2-(2-hydroxyphenyl)benzothiazole ligands. The

*Correspondence: abrahamke@gmail.com

This work is licensed under a Creative Commons Attribution 4.0 International License.

study claimed that the novel zinc complexes are good candidates for electron-transporting host materials in phosphorescent OLEDs [9]. Xie et al. conducted a study on the crystal structure, thermal stability, and optoelectronic properties of an azomethine-zinc complex for organic EL applications [10]. Yu et al. presented the structures, electronic states, and EL properties of a Zn(II) 2-(2-hydroxyphenyl)benzothiazolate ($Zn(BTZ)_2$) complex and asserted that the $Zn(BTZ)_2$ has better electron transport properties as compared to tris(8-hydroxyquinolinato)aluminum [11]. Zeng et al. examined the synthesis, characterization, and EL properties of (E)-2-(2-(9-p-tolyl-9H-carbazol-3-yl)vinyl)-8-hydroxyl-quinoline, (E)-2-(2-(9-(4-methoxyphenyl)-9H carbazol-3-yl)vinyl)-8-hydroxyquinoline, and their respective zinc(II) complexes for application in single-layer organic light-emitting diodes. They established that these Zn(II) complexes generally emit yellow light in OLEDs [12]. Based on these works, we conclude that the zinc complexes of $C_{18}H_{12}N_2O_2$ polymers are used mainly as electron-transporting and yellow emissive active layers for EL devices.

Generally, the electronic $\pi - \pi^*$ transitions between the highest occupied molecular orbital (HOMO) and the lowest unoccupied molecular orbital (LUMO) levels of 8-hydroxyquinoline ligands are localized on the phenoxide and pyridyl rings of the polymer chain, respectively [6]. As a result, a blue shift or a red shift luminescence emission could be produced from the normal band gap energy of the host 8-hydroxyquinoline polymer, owing to the nature of the incorporated organic or inorganic substituent [5,6]. Usually the emission wavelengths of Znq_2 can be tuned by modifying or varying the 2nd, 5th, or 7th position of the 8-hydroxyquinoline ring through the addition of electron-withdrawing or electron-donating organic or inorganic materials [6,7]. The present study scrutinizes the preparation of novel EL samples through the direct coupling of CuO and Fe_2O_3 nanomaterials into the parent/host $C_{18}H_{12}N_2O_2Zn$ polymer matrix. As a result, a broad green EL emission arises, which confirms a blue shift in the EL emission of prepared samples as compared with the luminescence emission of the host $C_{18}H_{12}N_2O_2Zn$ polymer matrix. To the best of our knowledge, the EL properties of CuO and Fe_2O_3 embedded $C_{18}H_{12}N_2O_2Zn$ polymer electroluminor samples have not been reported yet. This study confirms the successful incorporation of CuO and Fe_2O_3 nanomaterials into the host $C_{18}H_{12}N_2O_2Zn$ polymer matrix through structural, molecular, and morphological analysis. The material composition and the presence of oxidized metal ions in the samples are clearly verified through X-ray photoelectron spectroscopic (XPS) analysis. The green EL emission in the present samples signifies the potential of the prepared materials not only for EL devices but also for lighting applications.

2. Materials and methods

The 99.99% pure $C_{18}H_{12}N_2O_2Zn$, CuO, and Fe_2O_3 starting materials were directly purchased from Sigma-Aldrich and used without any further purification. For the synthesis of the $C_{18}H_{12}N_2O_2Zn$:CuO electroluminor polymer composite, $C_{18}H_{12}N_2O_2Zn$, and CuO were taken in the weight ratio of 1:0.5 and mixed thoroughly using an agate mortar for 1 h. The obtained mixture was then annealed at 300 °C for 2 h in a quartz tubular furnace under Ar atmosphere with a rise in temperature at a rate of 5 °C/min. After annealing, the sample was cooled slowly to room temperature. The $C_{18}H_{12}N_2O_2Zn$:Fe_2O_3 electroluminor polymer composite was prepared using $C_{18}H_{12}N_2O_2Zn$ and Fe_2O_3 as starting materials through the same procedure adopted for the preparation of $C_{18}H_{12}N_2O_2Zn$:CuO composites. For further analysis, the samples $C_{18}H_{12}N_2O_2Zn$:CuO and $C_{18}H_{12}N_2O_2Zn$:Fe_2O_3 are referred to as CH and FH, respectively.

3. Characterizations

The structural and molecular verifications of the prepared samples were carried out using a Rigaku MiniFlex 600 X-ray diffractometer and PerkinElmer Spectrum Two FTIR spectrometer, respectively. The UV-Vis optical

absorption spectroscopy and photoluminescence (PL) spectroscopic analyses were conducted with an Agilent Cary 60 UV-Vis spectrometer and PerkinElmer LS45 PL spectrometer, respectively. The surface morphological studies were carried out using a field emission scanning electron microscopy (FESEM) instrument, model Nova Nanosem 450, and a high-resolution transmission electron microscopy (HRTEM) instrument, model JEOL JSM 2100, respectively. The BrukerXFlash 6 | 10 EDS detector equipped with the Nova Nanosem 450 FESEM instrument was used for materials composition analysis. The elemental characterization and the oxidation states of the elements involved in both samples were characterized by XPS analysis using an instrument from Kratos Analytical, UK. For EL spectra analysis, the prepared samples were sandwiched within two conducting electrodes. For applying a suitable forward biasing voltage to the sample, the transparent conducting indium tin oxide (ITO) coated on PET substrate was taken as the anode and an aluminum electrode was taken as the cathode. For the preparation of EL cells, the obtained powdered samples were mixed in AB glue epoxy and then spin-coated on ITO sheets. The aluminum cathode electrode was then attached on the opposite side of the sample. The EL emission from the sample through the ITO sheet was recorded using a computer-interfaced optical fiber attached to a spectrometer detector, model USB4000, from Ocean Optics.

3.1. Structural analysis

The XRD patterns of CH and FH samples are presented in Figures 1a and 1b, respectively. They show the distinguished peaks of metal oxide and polymer materials, which signify the successful formation of the polymer-metal oxide nanocomposite through the present synthesis route. In Figure 1a, the peaks at 2θ values of 32.62°, 35.66°, 38.82°, 48.98°, 53.54°, 58.32°, 61.72°, 65.9°, 66.42°, 68.18°, 72.46°, and 75.32° are due to the reflections from (110), (11^{-}1), (111), (20^{-}2), (020), (202), (11^{-}3), (022), (310), (220), (311), and (222) planes of CuO. These characteristic peaks of CuO are agreement with JCPDS file no. 48-1548 and confirm the presence of the monoclinic crystal system of CuO with lattice parameters a = 4.68, b = 3.42, c = 5.13, and β = 99.50. The peaks at 16.06°, 16.56°, 18.30°, 21.01°, and 29.09°indicate the presence of $C_{18}H_{12}N_2O_2Zn$ in the nanocomposite, which is confirmed by comparing the peaks with the standard JCPDS card no. 48-2116. In Figure 1b, the peaks at 24.12°, 33.13°, 35.58°, 40.90°, 49.51°, 54.10°, 57.58°, 62.40°, and 64.04° correspond to the reflections from the lattice planes (012), (104), (110), (113), (024), (116), (112), (214), and (300) of Fe_2O_3 (JCPDS card no. 88-0866) having a rhombohedral crystal system with lattice parameters a = 5.03 and c = 13.74. Similar peaks are observed for $C_{18}H_{12}N_2O_2Zn$ in the FH sample. The XRD study of both samples authenticates the presence of CuO and Fe_2O_3 metal oxide in the $C_{18}H_{12}N_2O_2Zn$ polymer material and also corroborates the successful incorporation of these metal oxides into $C_{18}H_{12}N_2O_2Zn$ at 300 °C.

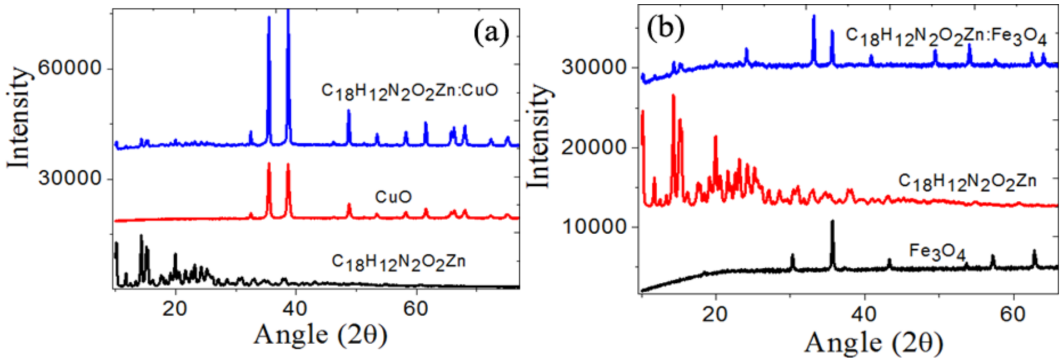

Figure 1. XRD patterns: (a) sample CH and (b) sample FH.

3.2. Optical absorption analysis

The UV-Vis absorption spectra of CH and FH are given in Figures 2a and 2b, respectively. In both samples, there are multiple absorption regions, which indicates the polymeric nature of the sample, particle size inhomogeneities, and the occurrence of large numbers of metal/oxygen ions and metallic/oxygen vacancies in the prepared samples [13–15]. Broad absorption peaks centered at 2.96 eV for CH and 2.63 eV for FH, respectively, are observed clearly in Figures 2a and 2b. Generally the metal complexes of quinoline polymers show an intense absorption peak at about 4.8 eV due to $\pi \rightarrow \pi^*$ transition of quinoline and a low intensity peak at about 3.2 eV due to $n \rightarrow \pi^*$ transition of the N atom of the quinoline ring [5,6]. Hence, it could be understood that the observed broad absorption peaks for the present samples are due to the formation of coordinate bonds between $C_{18}H_{12}N_2O_2Zn$ and CuO and Fe_2O_3 metal oxides in CH and FH samples, respectively, which again confirms the better coordination of $C_{18}H_{12}N_2O_2Zn$ with CuO and Fe_2O_3 metal oxides. The average optical band gap energies for CH and FH are calculated by fitting the experimental data using the theoretical equation $(\alpha h\upsilon)^{1/n} = B(h\upsilon - E_g)$, where B is a constant and E_g is the optical band gap, and exponent n depends on the type of transitions. If n = 1/2, the equation is for allowed direct transition, and if n = 2, it is for indirect transitions. The band gap energies obtained for the CH and FH samples are 2.30 eV and 2.01 eV, respectively.

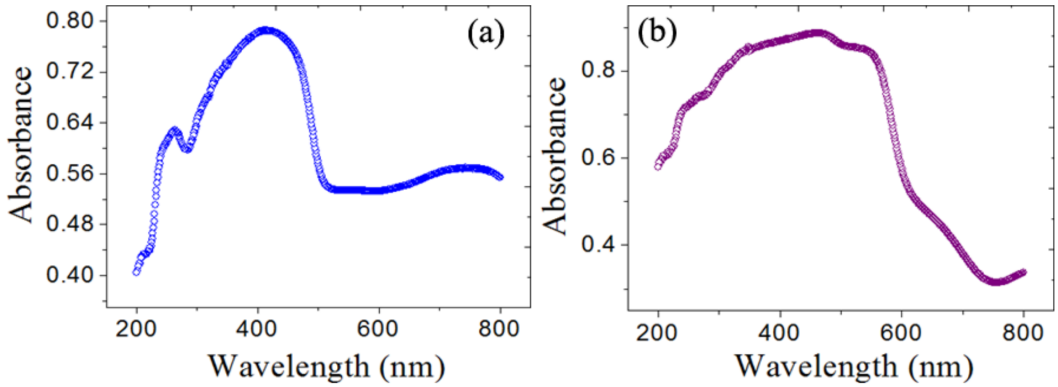

Figure 2. UV-Vis absorption spectra: (a) sample CH and (b) sample FH.

3.3. Molecular analysis

Figures 3a and 3b show the molecular bond vibrations of CH and FH samples, respectively, in FTIR spectroscopic analysis. The results are compared with previous reports and it is observed that the vibration levels match well with the previous results [16–18]. The FTIR vibrations and respective assignments are given in the Table. It is recognized that the FTIR results are in agreement with the results obtained from the XRD analysis of both CH and FH samples.

3.4. Morphological analysis

The FESEM and HRTEM images of prepared samples are presented in Figures 4a–4d. Figures 4a and 4c show the images for CH, while Figures 4b and 4d show those for FH. The FESEM images for both samples indicate that the surfaces of nanoparticles are very smooth and no beads or cracks are created on the surface. The exact shapes of the nanoparticles are not defined from the FESEM images. However, from the HRTEM images, the CH

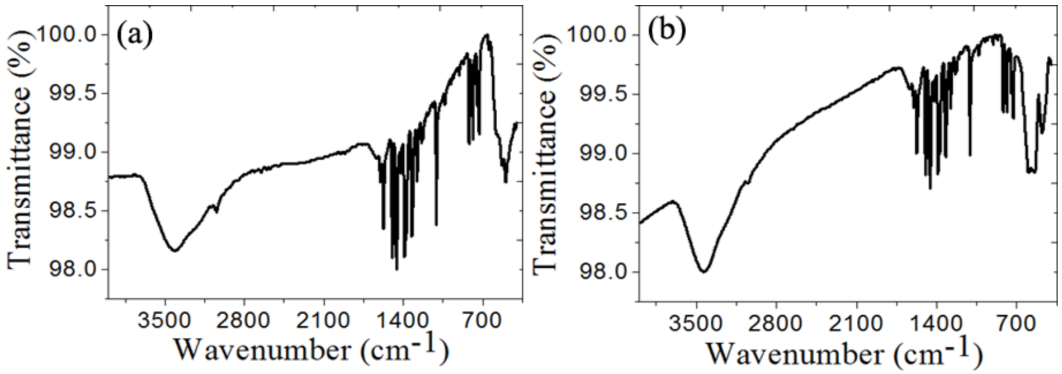

Figure 3. FTIR spectra: (a) sample CH and (b) sample FH.

Table. FTIR assignments of CH and FH samples.

CH (cm^{-1})	FH (cm^{-1})	Assignments
496	476 538 594	Metal oxide vibration such as Zn-O, Cu-O, and Fe-O
730–820	730–820	Plane ring deformations of 8-hydroxyquinoline zinc
1105 1276	1098 1271	C-O vibrational absorption peak
1321 1392	1319 1389	Vibrations of metallic bonding with quinoline molecules
1458 1500	1451 1500	Pyridyl and phenyl group vibrations of 8-hydroxyquinoline
1568	1575 1645	C=C and C=N skeletal stretching vibrations
3034–3408	3048–3443	O-H stretching vibrations

samples look spherical and the FH samples look like flakes. The HRTEM analysis of both samples reveals that the CuO and Fe_2O_3 metal oxides are completely surrounded by $C_{18}H_{12}N_2O_2Zn$ polymer, which is evident from the black regions (metal oxide) inside the white regions (polymer) of HRTEM images. It also confirms the better incorporation of the metal oxide and $C_{18}H_{12}N_2O_2Zn$ host polymer matrix. The EDS analysis results are given in Figures 5a and 5b for CH and FH samples, respectively. The EDS analysis confirms the presence of Cu, Zn, and C elements in the CH sample and Fe, Zn, and C in the FH sample. The compositional atomic weight percentages are presented in the insets of Figures 5a and 5b. The SAED patterns for both CH and FH are represented in Figures 5c and 5d. The SAED pattern indicates the polycrystalline nature of the prepared composites at 300 °C.

3.5. X-ray photoelectron spectroscopic analysis

The XPS analysis spectra of CH and FH samples are given in Figure 6. The wide scan spectra of CH and FH confirm the existence of the elements Cu, Fe, Zn, C, N, and O, which are in good agreement with elemental compositional analysis results from the EDS spectra. The high-resolution XPS deconvoluted Cu2p spectrum of CuO is presented in Figure 6a, which shows the presence of Cu^{2+} oxidation states of CuO in the CH sample. The strong fitted peaks at around 934.4 eV and 954.1 eV correspond to the oxidation states Cu^{2+} 2p3/2 and

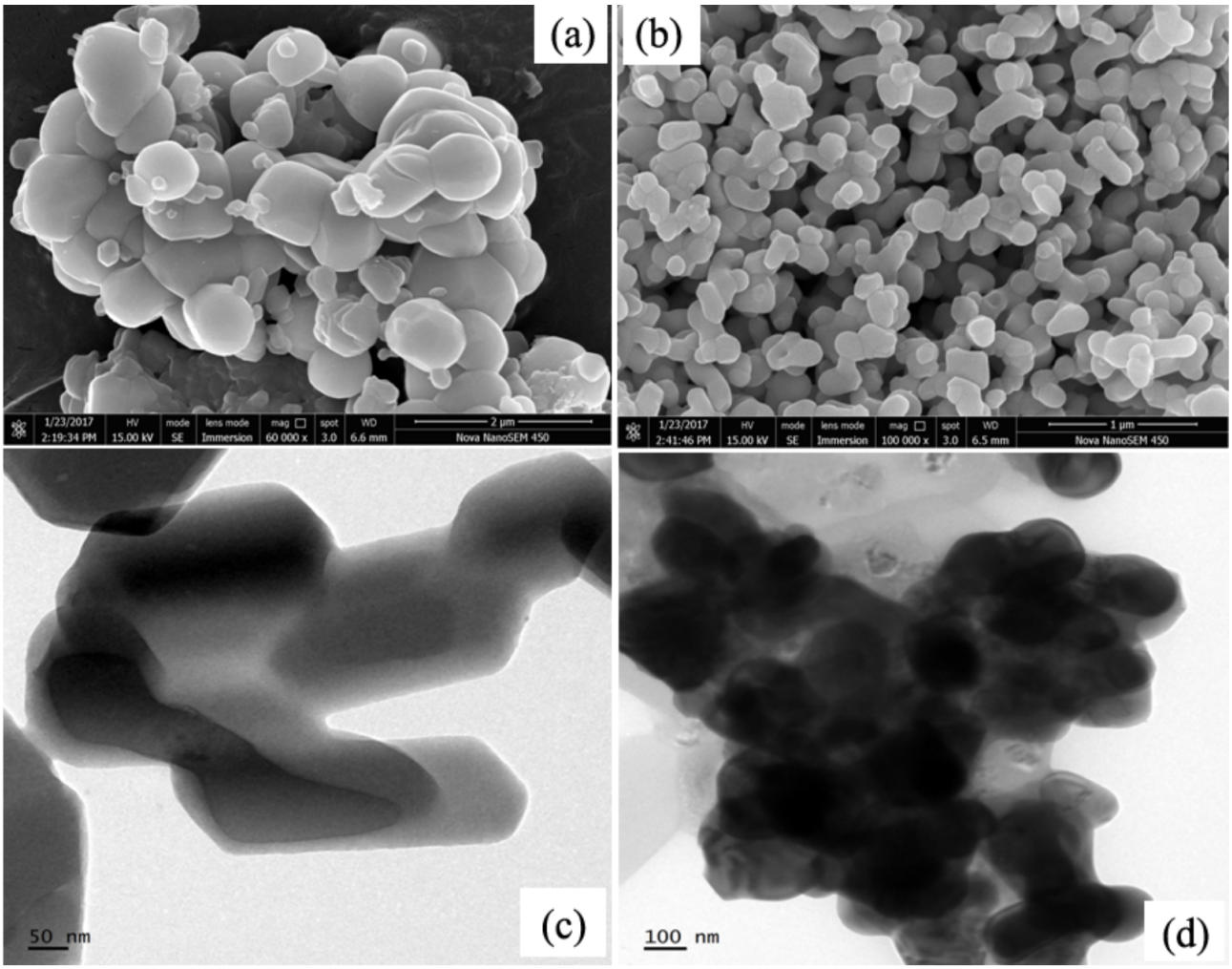

Figure 4. FESEM and TEM images: (a, c) FESEM and TEM images of the CH sample; (b, d) FESEM and TEM images of FH, respectively.

2p1/2 of CuO, respectively [19–21]. The binding energy value obtained for the present Cu^{2+} 2p3/2 is greater than that of CuO (933.8), which confirms that the CuO is surrounded by $C_{18}H_{12}N_2O_2Zn$ polymer material as seen in the TEM analysis of the samples. The binding energy gap obtained between the Cu2p3/2 and Cu2p1/2 states is 19.7 eV, which matches the standard value 20.0 eV of CuO [20–22]. In addition to these peaks, shake-up satellite peaks are observed at 940.6 eV and 943.5 eV, which are mainly due to an open $3d^9$ shell corresponding to Cu^{2+} states of Cu2p [23,24]. The high-resolution deconvoluted Fe2p spectrum of Fe_2O_3 existing in sample FH is given in Figure 6b. Two main peaks are situated around 710.6 eV and 724.1 eV, which correspond to Fe2p3/2 and Fe2p1/2, respectively, of the Fe^{3+} oxidation state of Fe_2O_3 [25–27]. Besides these peaks, a shake-up satellite peak is located at 718.4 eV, which again supports the assertion that Fe existed in the Fe^{3+} ionic state. The binding energy gap obtained between Fe2p3/2 and Fe2p1/2 states is 13.5 eV, which is very close to the normal value of Fe_2O_3 [28,29].

The deconvoluted XPS spectra for C1s, Zn2p, and O1s are observed to be similar for the CH and FH samples, which strongly supports the successful incorporation of CuO and Fe_2O_3 compounds in the

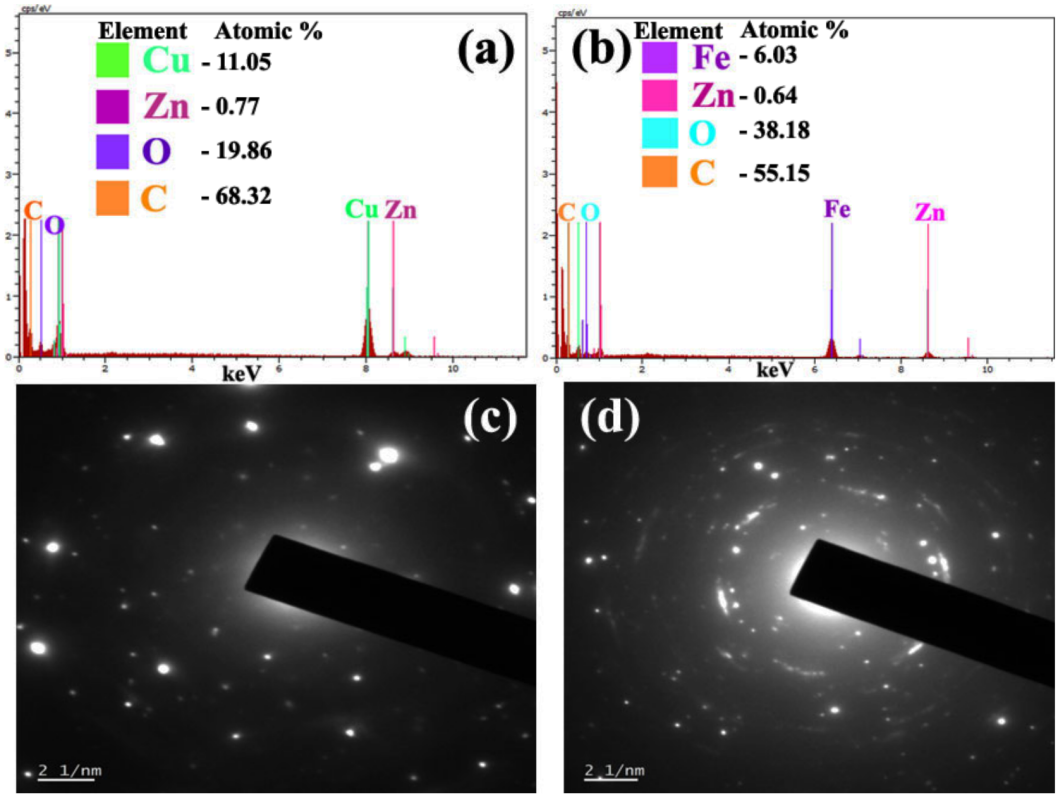

Figure 5. EDS and SAED patterns: (a, c) EDS and SAED patterns of the CH sample; (b, d) EDS and SAED patterns of FH, respectively.

$C_{18}H_{12}N_2O_2Zn$ polymer. Figure 6c shows the intense nature of the C1s peak, which confirms the occurrence of carbon in both CH and FH nanocomposite samples. The most intense peak at 284.7 eV demonstrates the C-C bonding. The binding energy for the chemical states of C-OH and C-O-C lies at about 286.8 eV [21,22]. The peaks observed at 287.7 eV and 288.5 eV are assigned as carbon present in the nitrogen group of $C_{18}H_{12}N_2O_2$ (C-N-C) and O-C=O bonding energies, respectively [30,31]. This confirms the presence of carbon and nitrogen elements in CH and FH nanocomposite samples from $C_{18}H_{12}N_2O_2Zn$ polymer. The C1s binding energy peaks corresponding to C-C, C-OH, C-O-C, C-N-C, and O-C=O functional groups are in good agreement with the FTIR assignments of the prepared CH and FH samples. The inset of Figure 6c represents the deconvoluted oxygen O1s peak spectra for both samples. The lower binding energy at 529.7 eV is designated as O^{2-} in the nanocomposite structure [32–34]. The intermediate binding energy regions at 531.2 eV and 532.3 eV associated with O^{2-} ions exist mainly due to oxygen-deficient regions such as oxygen defects and oxygen interstitials occurring within the complex structures of CH and FH nanocomposites [31,32]. The higher binding energy region of the O1s spectrum at 533.6 eV is formed by the existence of chemisorbed oxygen ions on the surface of the nanocomposite complex structure [23–25]. The deconvoluted high-resolution XPS spectrum of Zn2p having two major peaks located at about 1021.4 eV and 1044.5 eV, respectively, is given in Figure 6d. The peaks at 1021.4 eV are assigned mainly as the Zn2p3/2 of the Zn^{2+} oxidation state [33–37], which indicates free Zn/Zn atoms that are not bonding with any other species in the complex structure of the CH and FH samples. The peak at 1044.5 eV is typically the Zn2p1/2 of the Zn^{2+} oxidation state [35–39]. The binding energy gap obtained between the Zn2p3/2 and Zn2p1/2 states is 23.1, which is quite close to the standard value [37–41].

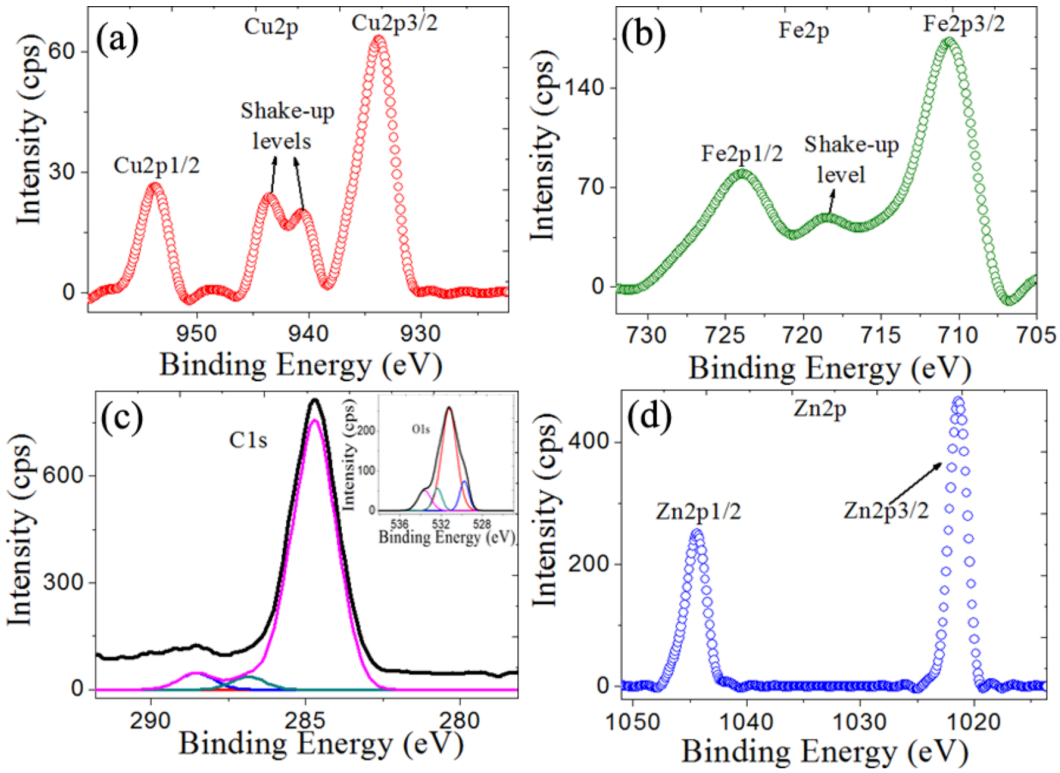

Figure 6. Deconvoluted XPS peaks of (a) Cu2p of CH, (b) Fe2p of FH; (c), (d), and inset of (c) corresponding to C1s, Zn2p, and O1s for CH and FH, respectively.

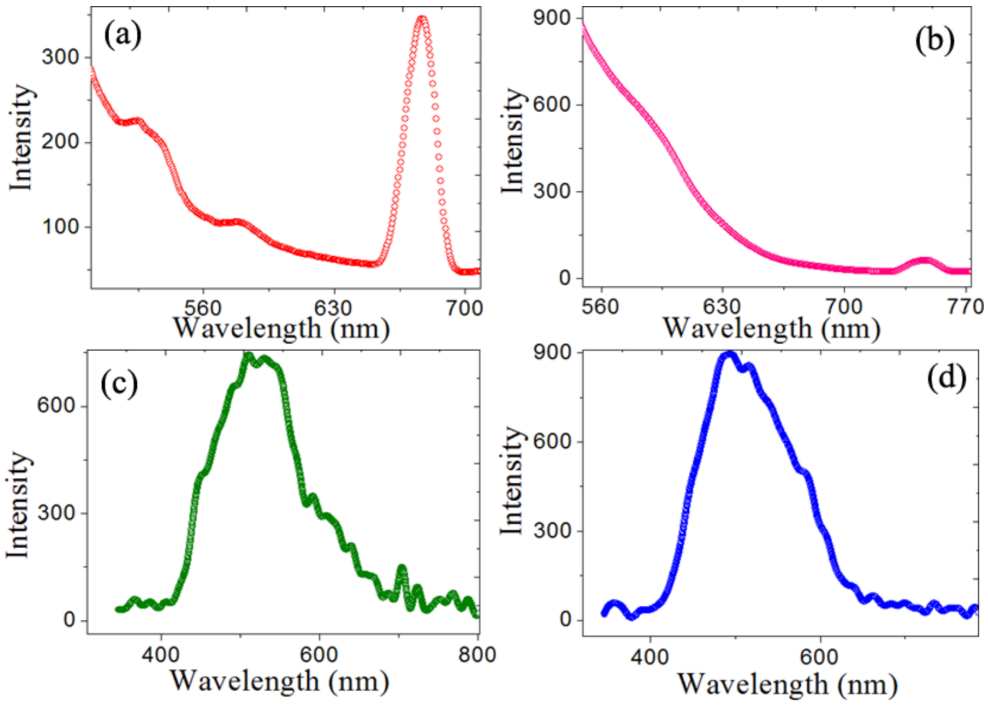

Figure 7. Photoluminescence and EL spectra: (a) and (c) for CH and (b) and (d) for FH.

3.6. Photoluminescence and EL analysis

The room temperature photoluminescence and EL spectra of the CH and FH samples are given in Figure 7. Figures 7a and 7b represent the photoluminescence spectrums of CH and FH samples at excitation wavelengths of 500 nm and 550 nm, respectively. The PL emission in metal complexes of quinoline polymers mainly occurs due to the HOMO level electronic transition from the electron-rich phenoxide ring to the electron-deficient pyridyl ring located at the LUMO level [11,12,42]. The FTIR analysis of the prepared nanocomposites reveals the presence of the pyridyl and phenyl group in the samples. Hence, the green PL emission observed at 2.36 eV in Figure 7a and at 2.15 eV in Figure 7b in the present samples is considered as band edge PL emission originating from the $C_{18}H_{12}N_2O_2Zn$ polymer material of the CH and FH nanocomposites [5–9]. The high and intense PL emission peak at 1.83 eV observed in Figure 7a originates from the intermediate level, within the HOMO-LUMO energy gap of CH. The PL emission peak at 1.65 eV detected in Figure 7b is also considered as intermediate level emission in the FH sample. Usually it originates from interstitial metal/oxygen ions or vacancies within the HOMO-LUMO gap. Sometimes the intensity of the intermediate level emission is much higher than that of the band edge or near the band edge emission [43–46]. In certain materials, numerous metal/oxygen ions and vacancies are created due to the various coordination mechanisms between the different molecules during sample formation [43–45]. These ionic oxidation states strongly restrict the easy movement of electrons from LUMO level to HOMO level during the photo/electroexcitation and therefore the electrons can be confined in such intermediate centers. Therefore, in certain situations, the density of electrons in the intermediate level is much higher than that in the excited HOMO level. Hence, the luminescence emissions originating from such centers can be more intense than band edge or near band edge luminescence emissions. The XPS analysis of the CH and FH samples (Figure 6) clearly confirms the presence of numerous oxidation states such as Cu^{2+}, O^{2-}, and Zn^{2+} in CH and Fe^{2+}, O^{2-}, and Zn^{2+} in FH samples. Hence, the obtained higher wavelength PL emissions are considered as the PL emissions originating from the intermediate oxidation centers present within the HOMO-LUMO energy gap of prepared samples.

The EL spectra of CH and FH samples are given in Figures 7c and 7d. Generally, the metal complexes of quinoline polymers, especially Zn/Al complexes of quinoline, are used for the production of red or yellow luminescence organic EL devices [7–12], but researchers invest more effort in creating attractive novel materials for producing luminescence emissions in the lower wavelength region of the visible spectrum for the production of white luminescence devices. The EL emission of sample CH is observed at 2.42 eV and the same for FH is at 2.45 eV. The broad EL emission centered in the mid-green region for CH and FH samples provides a clear picture of the generation of blue shift in EL emissions of both samples as compared with the normal EL emission behavior of Zn complexes of quinoline derivative polymers [5–12]. It was reported that the electron-donating groups and electron-withdrawing groups introduced into the metallic complexes of the quinoline ligand of organometallic electrolumophore can cause changes in electronic properties of the ligand involved in the emission of light [5,6]. Herein, the presence of CuO and Fe_2O_3 in the $C_{18}H_{12}N_2O_2Zn$ polymer can alter the luminescence behavior of the host polymer matrix. The exact interpretation of the change in EL emission behavior of prepared samples by the incorporation of CuO and Fe_2O_3 in the host polymer matrix is not well known. However, the interaction/coordination of metal oxide and polymer layers in the prepared sample is a crucial parameter for altering the optical performance of the host material.

Accordingly, the incorporation of CuO and Fe_2O_3 with $C_{18}H_{12}N_2O_2Zn$ produces a large amount of intermediate oxidation states such as Cu^{2+}, O^{2-}, and Zn^{2+} in CH and Fe^{2+}, O^{2-}, and Zn^{2+} in FH samples,

respectively. As stated earlier, the XPS analysis of the present samples evidently confirms the occurrence of such oxidation states in the prepared samples. The presence of oxidized metal/oxygen ions in these samples increases the size of the particles, which is confirmed by the larger particle size observed in the present HRTEM analysis. Occasionally this may be changed by the effective band energy of the present host polymer, which is presented in Figure 8. Besides this argument, the density of excited electrons in the intermediate level is greater than that of the excited electrons present in the conduction levels, which is confirmed by the origin of intense PL emission in the compounds. Therefore, the present study strongly suggests that the effective band energy of the prepared samples is shifted to the lower wavelength region through the averaging effect of the band gaps between the host polymer and incorporated foreign metal oxides in the samples. Hence, the present EL emission does not originate from the corresponding band edge/near band edge energies of the host polymer or incorporated foreign metal oxides in the samples. It originates from the new averaged band energy created between the band energies of the host polymer and incorporated foreign metal oxides. Hence, it is concluded that the blue shifted green EL emission in both CH and FH samples as compared with the host $C_{18}H_{12}N_2O_2Zn$ polymer matrix should be attributed to the shift in the band gap energy of the host $C_{18}H_{12}N_2O_2Zn$ polymer matrix due the incorporation of CuO and Fe_2O_3 in the polymer matrix. Thus, it is logical to conclude that the substitution of appropriate metal oxide semiconductors in metal chelates would result in variation in the HOMO-LUMO energy gap and that could provide effective color tuning in semiconducting polymer EL materials.

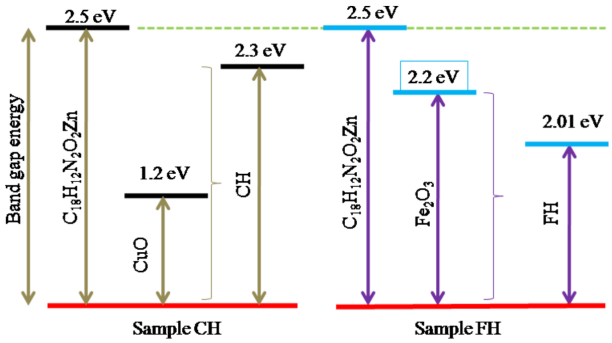

Figure 8. Band gap diagram of the CH and FH samples.

4. Conclusions

In summary, the present study confirms the successful formation and EL properties of CuO and Fe_2O_3 embedded $C_{18}H_{12}N_2O_2Zn$ polymer nanocomposites. The PL and EL analysis confirms that the prepared samples are suitable candidates for use in modern electronic display devices as well as in lighting applications. The present study also suggests an idea for band gap tuning of luminescent materials by incorporating the semiconductor metal oxides through the creation of numerous oxidation states. The present XPS analysis shows the presence of such oxidation states of Cu^{2+}, Fe^{2+}, Zn^{2+}, O^{2-}, C, and N via the incorporations of CuO and Fe_2O_3 in $C_{18}H_{12}N_2O_2Zn$ of $C_{18}H_{12}N_2O_2Zn$:CuO and $C_{18}H_{12}N_2O_2Zn$:Fe_2O_3 samples. The TEM analysis shows better inclusion of CuO and Fe_2O_3 in $C_{18}H_{12}N_2O_2Zn$ polymer materials. The XRD and FTIR analysis reveals the sample formation and molecular bonding between the $C_{18}H_{12}N_2O_2Zn$ polymer materials and CuO and Fe_2O_3. The EDS spectral analysis shows the presence of metal, oxygen, and polymer material compositions in the prepared samples.

Acknowledgment

The authors thank the Kerala State Council for Science, Technology, and Environment (KSCSTE) for providing the financial assistance for the present work.

References

[1] Qian-Huo C, Qing LQ, Li YS, Wen-Gong Z. Study on the structure and luminescence properties of the coordinated ZnO crystallites. Applied Physics A 2013; 113 (1): 135-143. doi: 10.1007/s00339-012-7500-7

[2] Bharathi DV, Rulmozhichelvan PA, Urugakoothan P. Synthesis and characterization of poly ethylene capped bis-(8 hydroxy quinoline) zinc nanoparticles. Asian Journal of Chemistry 2016; 28 (4): 779-781. doi: 10.14233/ajchem.2016.19476

[3] Ouyang X, Zeng H, Xie Y. Synthesis and photoluminescence properties of 8-hydroxyquinoline derivatives and their metallic complexes. Frontiers of Chemistry in China 2007; 2 (4): 407-413. doi: 10.1007/s11458-007-0077-6

[4] Taiju T, Yosuke N, Yasuko T. Photoluminescence of bis(8-hydroxyquinoline) zinc (Znq_2) and magnesium (Mgq_2). Central European Journal of Physics 2012; 10 (2): 524-528. doi: 10.2478/s11534-011-0090-8

[5] Debjit D, Vibha T, Suman CK, Shukla VK, Kumar S. Optical properties of electroluminescent zinc (IIbis(8-hydroxyquinoline) thin films prepared at different deposition rates. In: Proceedings of ASID '06; New Delhi, India; 2006. pp. 206-209.

[6] Jain VK, Abhishek V. Physics of Semiconductor Devices. Environmental Science and Engineering Environmental Science and Engineering Series. Cham, Switzerland: Springer, 2014.

[7] Yanping H, Jiguo L, Tanhua L, Xiaoming F, Xinhua O et al. Comparative studies on OLED performances of chloro and fluoro substituted Zn(II) 8-hydroxyquinolinates. New Journal of Chemistry 2015; 39 (1): 333-341. doi: 10.1039/C4NJ01085J

[8] Sapochak LS, Benincasa FE, Schofield RS, Baker JL, Riccio KK et al. Electroluminescent zinc(II) bis(8-hydroxyquinoline): structural effects on electronic states and device performance. Journal of American Chemical Society 2002; 124 (21): 6119-6125. doi: 10.1021/ja0201909

[9] Renjie W, Lijun D, Min F, Jinling C, Jiuyan L. Novel Zn (II) complexes of 2-(2-hydroxyphenyl)benzothiazoles ligands: electroluminescence and application as host materials for phosphorescent organic light-emitting diodes. Journal of Material Chemistry 2012; 22 (44): 23454-23460. doi: 10.1039/C2JM34599D

[10] Junfeng X, Juan Q, Liduo W, Jing X, Yong Q. An azomethin-zinc complex for organic electroluminescence: Crystal structure, thermal stability and optoelectronic properties. Inorganica Chimica Acta 2005; 358: 4451-4458. doi: 10.1016/j.ica.2005.08.018

[11] Gui Y, Shiwei Y, Yunqi L, Zhigang S, Daoben Z. Structures, electronic states, and electroluminescent properties of a zinc(II) 2-(2-hydroxyphenyl) benzothiazolate complex. Journal of American Chemical Society 2003; 125 (48): 14816-14824. doi: 10.1021/ja0371505

[12] Zeng HP, Wang GR, Zeng GC, Li J. The synthesis, characterization and electroluminescent properties of zinc(II) complexes for single-layer organic light-emitting diodes. Dyes and Pigments 2009; 83 (2): 155-161. doi: 10.1016/j.dyepig.2009.03.003

[13] Litty I, Nampoori VPN, Radhakrishnan P. Size dependent fluorescence spectroscopy of nanocolloids of ZnO. Journal of Applied Physics 2007; 102 (6): 063524-063530. doi: 10.1063/1.2778637v

[14] Litty I, Bindu K, Deepthy A, Nampoori VPN, Radhakrishnan P. Excitation wavelength dependent fluorescence behaviour of nano colloids of ZnO. Journal of Physics D: Applied Physics 2007; 40 (18): 5670-5676. doi: 10.1088/0022-3727/40/18/023

[15] Paulose T, Abraham KE. Excitation wavelength dependent visible photoluminescence of CdO nanomorphotypes. Journal of Luminescence 2015; 158: 422-427. doi: 10.1016/j.jlumin.2014.10.023

[16] Nagpure IM, Duvenhage MM, Pitale SS, Ntwaeaborwa OM, Terblans JJ et al. Synthesis, thermal and spectroscopic characterization of Caq2 (calcium 8-hydroxyquinoline) organic phosphor. Journal of Fluorescence 2012; 22 (5): 1271-1279. doi: 10.1007/s10895-012-1069-6

[17] Samia KA, Ghalia AZ, Mohamed AS. Removal of heavy metals from aqueous solutions by multi-walled carbon nanotubes modified with 8-hydroxyquinoline. Chemical Engineering Journal 2012; 181: 159-168. doi: 10.1016/j.cej.2011.11.044

[18] Qian-Huo C, Qing L, Qing L, Yu S, Wen-Gong Z. Study on the structure and luminescence properties of the coordinated ZnO crystallites. Applied Physics A 2013; 113 (1): 135-143. doi: 10.1007/s00339-012-7500-7

[19] Anita SE, Dae JK. Synthesis and characterization of CuO nanowires by a simple wet chemical method. Nano Research Letters 2012; 7 (70): 1-5. doi: 10.1186/1556-276X-7-70

[20] Daqiang G, Jing Z, Jingyi Z, Jing Q, Zhaohui Z et al. Vacancy-mediated magnetism in pure copper oxide nanoparticles. Nano Research Letters 2010; 5 (4): 769-772. doi: 10.1007/s11671-010-9555-8

[21] Chengli H, Jing O, Huaming Y. CuO nanoparticles encapsulated inside Al-MCM-41 mesoporous materials via direct synthetic route. Scientific Reports 2014; 4: 1-9. doi: 10.1038/srep03682

[22] Dmytro KS, Ruslan SA, Etsuro S, Atsushi I, Takashi N. Non-electrolytic synthesis of copper oxide/carbon nanocomposite by surface plasma in super-dehydrated ethanol. Scientific Reports 2016; 6: 1-9. doi: 10.1038/srep21178

[23] Stadnichenko AI, Sorokin AM, Boronin AI. XPS, UPS, and STM studies of nanostructured CuO films. Journal of Structural Chemistry 2008; 49 (2): 341-347. doi: 10.1007/s10947-008-0133-1

[24] Wu CK, Yin M, O'Brien S, Koberstein JT. Quantitative analysis of copper oxide nanoparticle composition and structure by X-ray photoelectron spectroscopy. Chemistry of Materials 2006; 18 (25): 6054-6058. doi: 10.1021/cm061596d

[25] Amir A, Bunyod A, Jeonghwan L, Heung WJ, Soon WJ et al. X-ray photoelectron spectroscopy characterization of Fe doped TiO_2 photocatalyst. International Journal of Material, Mechanics and Manufacturing 2013; 1 (3): 294-296. doi: 10.7763/IJMMM.2013.V1.63

[26] Basavaraja S, Balaji DS, Mahesh BD, Raghunandan D, Prithviraj Swamy PM et al. Solvothermal synthesis and characterization of acicular α-Fe_2O_3 nanoparticles. Bulletin of Material Science 2011; 34 (7): 1313-1317.

[27] Garcia D, Picasso G, Hidalgo P, Peres HEM, Kou RS et al. Sensors based on Ag-loaded hematite (α-Fe_2O_3) nanoparticles for methyl mercaptan detection at room temperature. Analytical Chemistry Research 2016; 23: 74-81. doi: 10.1016/j.ancr.2016.12.001

[28] Willis AL, Turro NJ, O'Brien S. Spectroscopic characterization of the surface of Iron oxide nanocrystals. Chemistry of Materials 2005; 17 (24): 5970-5975. doi: 10.1021/cm051370v

[29] Mohammed RM, Abdullah AM. Development of ionic-sensor based on sono-chemically prepared low-dimensional b-Fe_2O_3 nanoparticles onto flat-gold electrodes by an electrochemical approach. Sensors and Bio-Sensors Research 2015; 4: 109-117. doi: 10.1016/j.sbsr.2015.05.001

[30] Yanqing W, Bunshi F, Zhipeng W, Wei G, Ichiro S et al. Nitrogen-doped porous carbon monoliths from polyacrylonitrile (PAN) and carbon nanotubes as electrodes for supercapacitors. Scientific Reports 2017; 7 (40259): 1-10. doi: 10.1038/srep40259

[31] Vinod V, Thekkae P, Miroslav Č. Green synthesis of copper oxide nanoparticles using gum karaya as a biotemplate and their antibacterial application. International Journal of Nanomedicine 2013; 8 (1): 889-898. doi: 10.2147/IJN.S40599

[32] Shelke PD, Rajbhoj AS, Nimase MS, Takate SJ Zaware BH et al. Electrochemical synthesis, characterization and evaluation of antioxidant activity of copper oxide nanoparticles. Research Journal of Chemical Sciences 2016; 6 (9): 43-48. doi: 10.1016/j.jiec.2015.06.021

[33] Vinod K, Swart HC, Ntwaeaborwa OM, Kroon RE, Terblans JJ et al. Origin of the red emission in zinc oxide nanophosphors. Materials Letter 2013; 101: 57-60. doi: 10.1016/j.matlet.2013.03.073

[34] Usman I, Rawat RS, Wang Y, Tan TL, Lee P et al. Alteration of Mn exchange coupling by oxygen interstitials in ZnO:Mn thin films. Applied Surface Science 2012; 258 (17): 6373-6378. doi: 10.1016/j.apsusc.2012.03.043

[35] Biesinger MC, Payne BP, Grosvenor AP, Lau LWM, Gerson AR et al. Resolving surface chemical states in XPS analysis of first row transition metals, oxides and hydroxides: Cr, Mn, Fe, Co and Ni. Applied Surface Science 2011; 257 (3): 2717-2730. doi: 10.1016/j.apsusc.2010.07.086

[36] Seokhwan B, Seungjun L, Youngbin K, Joohyun P, Seokyoon S et al. Photocurrent detection of chemically tuned hierarchical ZnO nanostructures grown on seed layers formed by atomic layer deposition. Nano Research Letters 2012; 7: 1-11. doi: 10.1186/1556-276X-7-290

[37] Fang Y, Zhong YL, Jin LC, Xiao YS, Xiao JL et al. Nanoscale zeolitic imidazolate framework-8 as a selective adsorbent for theophylline over caffeine and diprophylline. RSC Advances 2014; 4 (62): 33047-33054. doi: 10.1039/C4RA05293E

[38] Usman I, Rawat RS, Tan TL, Lee P, Chen R et al. Oxygen rich p-type ZnO thin films using wet chemical route with enhanced carrier concentration by temperature-dependent tuning of acceptor defects. Journal of Applied Physics 2011; 110 (9): 093522. doi: 10.1063/1.3660284

[39] Usman I, Tan TL, Lee P, Ramanujan RV, Fengji L et al. Enhanced ferromagnetic response in ZnO:Mn thin films by tailoring composition and defect concentration. Journal of Magnetism and Magnetic Materials 2013; 344: 171-175. doi: 10.1016/j.jmmm.2013.05.040

[40] Lupan O. Synthesis and characterization of ZnO nanowires for nanosensor applications. Material Research Bulletin 2010; 45 (8): 1026-1032. doi: 10.1016/j.materresbull.2010.03.027

[41] Kayaci F, Vempati S, Donmez I, Biyikli N, Uyar T. Role of zinc interstitials and oxygen vacancies of ZnO in photocatalysis: a bottom-up approach to control defect density. Nanoscale 2014; 6 (17): 10224-10234. doi: 10.1039/C4NR01887G

[42] Anita S, Devender S, Partap KS, Amit K, Kapoor S et al. Electroluminescent characteristics of bis(5-chloro-8-hydroxyquinolinato)-zinc(II) complex. Indian Journal of Chemistry 2010; 49A (4): 448-451. http://nopr.niscair.res.in/handle/123456789/7829

[43] Debnath B, Halder G, Bhattacharyya S. One-step synthesis, structural and optical characterization of self-assembled ZnO nanoparticle clusters with quench-induced defects. Science of Advanced Materials 2014; 6 (6): 1160-1169. doi.org/10.1166/sam.2014.1881

[44] Ruiz Peralta Mde L, Pal U, Zeferino RS. Photoluminescence (PL) quenching and enhanced photocatalytic activity of Au-decorated ZnO nanorods fabricated through microwave-assisted chemical synthesis. ACS Applied Materials & Interfaces 2012; 4 (9): 4807-4816. doi: 10.1021/am301155u

[45] Gong Y, Andelman T, Neumark GF, O'Brien S, Kuskovsky IL. Origin of defect-related green emission from ZnO nanoparticles: effect of surface modification. Nano Research Letters 2007; 2 (6): 297. doi: 10.1007/s11671-007-9064-6

[46] Puja G, Manju A. Mechanism of photoluminescence enhancement and quenching in Nd_2O_3 nanoparticles–ferroelectric liquid crystal nanocomposites. RSC Advances 2015; 5 (20): 14974-14981. doi: 10.1039/C4RA14204G